A comparison between a centralised multilayer LPV/$\mathcal{H}\infty$ and a decentralised multilayer sliding mode control architectures for vehicle's global chassis control

Abbas Chokor, Reine Talj, Moustapha Doumiati, Ali Hamdan, Ali Charara

A comparison between a centralized multilayer $LPV\,/\,\mathscr{H}_\infty$ and a decentralized multilayer sliding mode control architectures for vehicle's global chassis control

Abbas Chokor[a], Reine Talj[a], Moustapha Doumiati[b], Ali Hamdan[a], and Ali Charara[a]

[a]Sorbonne universités, Université de Technologie de Compiègne, CNRS, Heudiasyc UMR 7253, CS 60 319, 60 203 Compiègne, France; [b]ESEO-IREENA EA 4642, 10 Bd Jeanneteau, 49100 Angers, France.

ARTICLE HISTORY
Compiled June 29, 2020

ABSTRACT
This paper investigates new achievements in global chassis control, involving Active Front steering (AFS) and Direct Yaw Control (DYC), to improve the overall vehicle performance, i.e. the vehicle maneuverability, lateral stability and rollover avoidance, in different driving situations. Two multilayer control architectures, each formed by three hierarchical layers, are developed, validated and compared. The lower layer represents the actuators implemented into the vehicle which generate their control inputs based on the orders sent from the middle layer. The middle layer is the control layer which is responsible to generate the control inputs that minimize the errors between the desired and actual vehicle yaw rate, side-slip angle, and roll angle, regardless of the driving situation. The control layer is the main difference of the proposed architectures, where a centralized and a decentralized controllers are developed. In the centralized architecture, the novelty with respect to other works in the field of chassis control is that one single Multi-Input-Multi-Output MIMO optimal controller generates the optimal additive steering angle provided by the AFS and the optimal differential braking provided by the DYC to minimize -at once- all the vehicle state errors (yaw rate, side-slip angle, and roll angle). The optimal $\mathscr{H}_\infty$ control technique based on offline Linear Matrix Inequality (LMI) optimal solutions, in the framework of Linear-Parameter-Varying (LPV) systems, is applied to synthesize the controller. In the decentralized architecture, a heuristic solution is proposed by decoupling the control problem where the Super-Twisting Sliding Mode (STSM) technique is applied to derive the AFS control input which minimizes only the errors on the yaw rate, and the roll angle. Similarly, the DYC control input is privileged to minimize only the error on the side-slip angle. The higher layer of both architectures is the decision making layer which instantly monitors two criteria laying on lateral stability and rollover risks. Then, it generates two weighted parameters which adapt the controller(s) dynamics and performance(s) according to the driving conditions in order to improve the vehicle's maneuverability, lateral stability and rollover avoidance. Both control architectures are tested and validated on the professional simulator "SCANeR Studio". Simulation shows that both architectures are relevant to the global chassis control. The centralized one is optimal, complex and overall closed-loop stability is guaranteed, while the decentralized one does not guarantee the overall closed-loop stability, but it is intuitive, simple, and robust.

KEYWORDS
$LPV\,/\,\mathscr{H}_\infty$ centralized control, sliding mode decentralized control, global chassis control.

CONTACT Chokor. Email: abbas.j.chokor@gmail.com

1. Introduction

1.1. Motivation

Driving safety is a major challenge for our society. According to the "National Highway Traffic Safety Administration (NHTSA)" statistics, human errors commit almost 90% of road accidents as explained in Rajamani (2012). The integration of an Advanced Driving Assistance System (ADAS) in the vehicle permits to act in an appropriate way to avoid accidents, skidding and rollover. ADAS systems are formed by several single-actuator approaches, such as: Electronic Stability Program (ESP) or Direct Yaw Control (DYC) to enhance the vehicle lateral stability; Active Front Steering (AFS) to mainly improve the vehicle maneuverability or lane keeping; and (Semi-)Active Suspensions (AS) to improve comfort (roll, pitch and heave motions attenuation), road holding and rollover avoidance.
In the objective of improving the global performance of the vehicle in different driving situations, more sophisticated chassis control systems are developed in literature to create synergies between several ADAS systems. These sophisticated controllers, known as Global Chassis Control (GCC) systems have to deal with the control of complex problems for Multi-Input-Multi-Output (MIMO) systems.

1.2. Related Works

The coordination between the AFS and the DYC to improve the vehicle maneuverability and lateral stability depending on the driving situation is one of the main tasks in GCC field. Several advanced control methods have been developed for this issue. In a decentralized approach, authors in He (2006) have developed a DYC controller for lateral stability purpose and an AFS controller for maneuverability purpose, based on sliding mode technique, and then a monitor switches between both stand-alone controllers according to the driving situations. Similarly, based on the fuzzy-logic technique, a coordination approach between AFS and DYC has been developed in Karbalaei (2007). However, the decentralized strategy does not guarantee the overall closed-loop stability of the system when switching between controllers or when both controllers are actuated simultaneously. Authors of Poussot-Vassal (2009), Doumiati (2013), and Doumiati (2014) have developed several robust and optimal MIMO centralized controllers based on LPV/$\mathscr{H}_\infty$ control technique, where the $LPV\,/\,\mathscr{H}_\infty$ controller penalizes or relaxes the steering and braking to enhance maneuverability and lateral stability. The overall closed-loop stability of the system is thus guaranteed, since the controllers' actuation is automated based on the polytopic approach. However, these controllers do not directly involve the vehicle roll motion and rollover problem in the controller synthesis. Some of them state the advantage on the rollover problem as a consequence of the controller without guaranteeing the rollover avoidance. From the other side, many recent research (centralized and decentralized) such as T. Vu (2017), Yao (2017), and Mirzaei and H. Mirzaeinejad (2017) propose to control the vertical load transfer, as a function of the roll angle and its angular velocity to avoid rollover. They also conclude the enhancements on lateral stability as a consequence. Nevertheless, these research require the integration of new actuators into the chassis like (semi-)active suspensions or active anti-roll bar. Authors of Sename (2013), Chen (2016) and Fergani (2013) have developed several powerful centralized $LPV\,/\,\mathscr{H}_\infty$ controllers, where the decoupled lateral and vertical vehicle dynamics are respectively controlled by the AFS+DYC and by the (semi-)active suspensions. Some other relevant research such as Ackermann and D. Odenthal (1998),Odenthal (1999), andSolmaz (2007) propose to control the roll motion by the steering and/or braking to avoid the rollover, regardless of the maneuverability and the vehicle trajectory.

All these interesting research have motivated us to study the control of the vehicle yaw rate, the side-slip angle and the roll angle to improve vehicle's maneuverability, lateral stability, and also rollover avoidance using only steering and braking actuators, by adopting both control architectures (centralized and decentralized).

1.3. Contribution

This work exposes the design and validation of two new (centralized and decentralized) multilayer control architectures to improve the vehicle maneuverability, the lateral stability and the rollover avoidance, using only steering and braking actuators.
This work contributions with respect to literature are:

- a new centralized control structure, which combines the yaw rate control, the side-slip angle control, and the roll control, in one single centralized controller, ensuring internal stability when switching between maneuverability, lateral stability and rollover avoidance objectives;
- a new decentralized control structure, which facilitates the global chassis control, by decoupling the control problem, into two sub-control problems, such as: AFS is responsible on the control of the yaw rate, and the roll angle; DYC is responsible on the control of the side-slip angle. Despite of the decoupling procedure, high maneuverability, lateral stability and rollover avoidance performances are guaranteed;
- a comparison between both approaches using SCNeR Studio simulator.

The paper structure is as the following: Section 2 exposes the extended bicycle model which combines the coupled lateral (yaw and side-slip) and roll motions. The lateral stability and rollover criteria, as the performance criteria used in this work, are also defined in the same section. Section 3 details the centralized and the decentralized control architectures. We present first an overview of both architectures applied to the vehicle dynamics and a general methodology of comparison between both architectures. Then, we present the detailed *MIMO LPV* $/\mathscr{H}_\infty$ centralized controller structure, as a model-based controller, we also detail the control objectives represented as variable-weighted filters, to finally find the *LPV* $/\mathscr{H}_\infty$ controller which guarantees $\mathscr{H}_\infty$ performances between the exogenous inputs and the controlled variables, based on offline LMI optimization, in the framework of the polytopic approach. Later on, we detail both AFS and DYC *STSM* controllers, as model-based controllers, where the control inputs are saturated and filtered a-posteriori. In the same section, the decision and the actuator layers of both the centralized and decentralized control architectures are presented. In Section 3.4, we test and validate both architectures on a simulation vehicle thanks to the co-simulation between Simulink and SCANeR Studio Simulator. Finally, in Section 5, we conclude on the achievements of this work, and provide a glance of our future work.

2. Vehicle dynamics

2.1. vehicle modeling

The vehicle is a complex system, whose behavior is strongly nonlinear. It contains several dynamical components such as wheels (acceleration, braking), steering system, suspensions, etc... which define the vehicle dynamics such as, lateral (yaw and side-slip), roll, pitch, heave and wheels motions, etc...(see Figure 1). A complete nonlinear vehicle model has already been developed and validated using the professional simulator "SCANeR Studio" Chokor

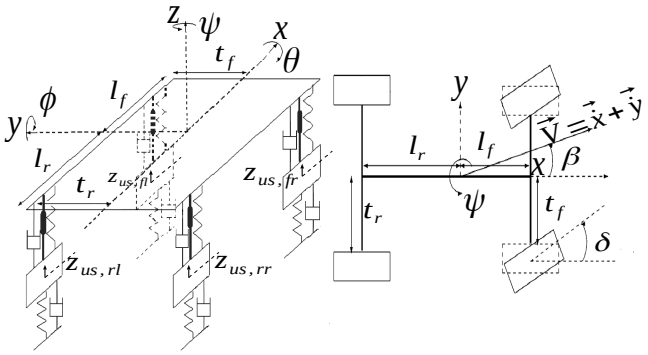

Figure 1.: Full vehicle model

(2016) and Chokor (2017). This model serves to understand the details of the vehicle dynamics by performing accurate simulations. However, this complex model does not suit the control problem formulation because of several real-time problems like unknown parameters, unavailable variables, and computational issues. Thus, a linear simplified vehicle model, which only combines the coupled lateral and roll motions is inspired from literature T. Vu (2017). This model suits the control problem of this work and it is given by the "*Plant P*" of the following system:

$$Plant\ P: \begin{cases} I_z\ddot{\psi} &= F_{yf}l_f + F_{yr}l_r + I_{xz}\ddot{\theta} + M_z + M_{d,\psi}, \\ M\mathrm{V}\left(\dot{\beta}+\dot{\psi}\right) &= F_{yf} + F_{yr} + M_s h_\theta \ddot{\theta} + F_{d,y}, \\ \left(I_x + M_s h_\theta^2\right)\ddot{\theta} &= M_s h_\theta \mathrm{V}\left(\dot{\beta}+\dot{\psi}\right) + (M_s g h_\theta - K_\theta)\theta \\ & \quad -C_\theta\dot{\theta} + M_{d,\theta}, \end{cases} \tag{1}$$

where $\dot{\psi}$, β, and θ are respectively the vehicle yaw rate, the vehicle side-slip angle, and the suspended mass roll angle. $M_{d,\dot{\psi}}, F_{d,y}, M_{d,\theta}$ represent the external disturbances and modeling errors respectively on the vehicle yaw rate, the lateral motion (side-slip angle) and the roll motion.M_z is the active yaw moment to be generated. F_{yf} represents the lateral force of the front left and right tires merged together at the center of the front axle. Similarly, F_{yr} is noted for the rear axle. The front and rear tires lateral forces F_{yf} and F_{yr} are supposed to be linear respectively to the front and rear tires side-slip angles α_f and α_r, such that:

$$\begin{aligned} F_{yf} &= \mu C_f \alpha_f, \\ F_{yr} &= \mu C_r \alpha_r, \end{aligned} \tag{2}$$

where C_f and C_r are the cornering stiffness of the front and rear tires. The tires slip angles α_f and α_r are given in the following equations:

$$\begin{aligned} \alpha_f &= -\beta - \tfrac{l_f\dot{\psi}}{V} + \delta_t, \\ \alpha_r &= -\beta + \tfrac{l_r\dot{\psi}}{V}, \end{aligned} \tag{3}$$

where $\delta_t = \delta_d + \delta_c$ is the total front wheel steering respectively composed by the driver steering and the active front steering angles. The remaining notations of these equations and the vehicle parameters used for simulation are given in Table 1. Even though these equations are valid when the vehicle operates in the stable region (no rollover or lateral stability risks), they are sufficient and recommended to synthesize a robust controller.

$$\dot{X} = \begin{bmatrix} \ddot{\psi} \\ \dot{\beta} \\ \dot{\theta} \\ \ddot{\theta} \end{bmatrix} = \underbrace{\begin{pmatrix} a_{11} & a_{12} & a_{13} & a_{14} \\ a_{21} & a_{22} & a_{23} & a_{24} \\ 0 & 0 & 0 & 1 \\ a_{41} & a_{42} & a_{43} & a_{44} \end{pmatrix}}_{A} \underbrace{\begin{bmatrix} \dot{\psi} \\ \beta \\ \theta \\ \dot{\theta} \end{bmatrix}}_{X} + \underbrace{\begin{pmatrix} b_{u,11} & b_{u,12} \\ b_{u,21} & b_{u,22} \\ 0 & 0 \\ b_{u,41} & b_{u,42} \end{pmatrix}}_{B_u} \underbrace{\begin{bmatrix} \delta_d + \delta_c \\ M_z \end{bmatrix}}_{U} + \underbrace{\begin{pmatrix} b_{d,11} & 0 & 0 \\ 0 & b_{d,22} & 0 \\ 0 & 0 & 0 \\ 0 & 0 & b_{d,43} \end{pmatrix}}_{B_d} \underbrace{\begin{bmatrix} M_{d,\psi} \\ F_{d,y} \\ M_{d,\theta} \end{bmatrix}}_{D}; \quad (4)$$

$$y = X.$$

$$\dot{X}_{bic} = \begin{bmatrix} \ddot{\psi}_{bic} \\ \dot{\beta}_{bic} \\ \dot{\theta}_{bic} \\ \ddot{\theta}_{bic} \end{bmatrix} = \underbrace{\begin{pmatrix} a_{11} & a_{12} & a_{13} & a_{14} \\ a_{21} & a_{22} & a_{23} & a_{24} \\ 0 & 0 & 0 & 1 \\ a_{41} & a_{42} & a_{43} & a_{44} \end{pmatrix}}_{A} \underbrace{\begin{bmatrix} \dot{\psi}_{bic} \\ \beta_{bic} \\ \theta_{bic} \\ \dot{\theta}_{bic} \end{bmatrix}}_{X_{bic}} + \underbrace{\begin{pmatrix} b_{u,11} \\ b_{u,21} \\ 0 \\ b_{u,41} \end{pmatrix}}_{B_{u,bic}} \underbrace{\begin{bmatrix} \delta_d \end{bmatrix}}_{U_{bic}}; \quad (5)$$

$$y = X.$$

By substituting (3) in (2), and then in (1), the state space representation of the *Plant P* can be formalized as in (4) (see next page), where $X = [\dot{\psi}, \beta, \theta, \dot{\theta}]^T$ is the state vector, $U = [\delta_c, Mz]^T$ is the vector of control inputs, $D = [M_{d,\dot{\psi}}, F_{d,y}, M_{d,\theta}]^T$ is the vector of exogenous inputs. The elements of the state matrix $A \in I\!R^{4\times4}$, and the input matrices $B_u \in I\!R^{4\times2}$ and $B_d \in I\!R^{4\times3}$ are formalized in Appendix A.

The output variables $\dot{\psi}$ and $\dot{\theta}$ are supposed to be measured and given at the CG of the vehicle, in real time control, by gyro-meters; θ is integrated from $\dot{\theta}$ (θ could be directly taken from the Inertial Measurement Unit IMU if available). The side-slip angle β (and its velocity $\dot{\beta}$) could be estimated. Several observer approaches that suit the real time constraints implementation and vehicle dynamics have been proposed in literature to estimate β, e.g. an Extended Kalman Filter EKF based observer as done in Chen (2016) and Doumiati (2012).

The extended linear bicycle model (5) (see next page) is similar to (4), while no control and exogenous inputs are considered ($\delta_c = M_z = M_{d,\dot{\psi}} = F_{d,y} = M_{d,\theta} = 0$), except the driver's one δ_d. Based on the vehicle speed V and the driver's steering angle δ_d, the extended bicycle model generates the "bicycle trajectory vector" $X_{bic} = [\dot{\psi}_{bic}, \beta_{bic}, \theta_{bic}, \dot{\theta}_{bic}]^T$. These trajectories are coherent to each other, feasible and represent the ideal stable states of the vehicle. Authors of Rajamani (2012) propose to saturate $\dot{\psi}_{bic}$, and β_{bic}, as described in (6), to maintain the adherence between the tires and the road. This issue is done here.

$$\begin{aligned} |\dot{\psi}_{bic}| &\leq 0.85\mu\ g/V_x, \\ |\beta_{bic}| &\leq arctan(\mu\ g). \end{aligned} \quad (6)$$

Without loss of similarity, the trajectories provided by the extended bicycle model are used as the reference trajectories in the centralized approach, while they are slightly modified in the decentralized approach in order to introduce the weighting parameters. This issue is more developed later.

2.2. Performance criteria

The criterion by which the lateral stability can be quantified is called "*lateral stability index*" *SI*. *SI* reflects the orientation of the vehicle w.r.t its speed vector at the *CG*, and its rate of change. The lateral stability index (*SI*) used in Chen (2016) is expressed in (7) as:

$$SI = \left| q_1\beta + q_2\dot{\beta} \right|, \quad (7)$$

Table 1.: Notations and Parameters Values for Simulation

Symbols	Description	Parameters values
i	$i = \{f : front, r : rear\}$	
j	$j = \{r : right, l : left\}$	
θ	Sprung mass roll angle	$[rad]$
ϕ	Sprung mass pitch angle	$[rad]$
$\dot{\psi}$	Vehicle yaw rate	$[rad/s]$
β	Vehicle side-slip angle at CG	$[rad]$
F_{y_i}	Lateral forces at the i axle	$[N]$
δ_d	Driver steering angle	$[rad]$
V	Vehicle speed	$[m/s]$
I_x	Roll moment of inertia of sprung mass	534 $[kg.m^2]$
I_z	Vehicle yaw moment of inertia	1970 $[kg.m^2]$
I_{xz}	Vehicle yaw-roll product of inertia	743 $[kg.m^2]$
h_θ	Sprung mass roll arm	0.27 $[m]$
M_s	Sprung mass weight	1126.4 $[kg]$
M	Vehicle weight	1286 $[kg]$
t_r	Half rear track	0.773 $[m]$
l_f	Wheelbase to the front	1.0385 $[m]$
l_r	Wheelbase to the rear	1.6015 $[m]$
g	Gravity constant	9.81 $[m/s^2]$
μ	Road adherence coefficient	dry surface= 1 $[-]$
C_f, C_r	Front, rear tire cornering stiffness	76776 $[N/rad]$
K_θ	Roll suspension angular stiffness	30000 $[N.m/s]$
C_θ	Roll suspension angular damper	10000 $[N.m/s]$

where q_1 and q_2 are identified depending on the vehicle parameters and road adherence. SI varies between 0 and 1. For $SI \leq \underline{SI}$ (a predefined lower threshold depending on the vehicle and road parameters), the vehicle is in normal driving situations. When the vehicle reaches critical lateral stability, The lateral stability index SI becomes bigger than a predefined higher threshold $\overline{SI}$ ($SI \geq \overline{SI}$).
The criterion by which the rollover risk is evaluated is called "Load Transfer Ratio" LTR. LTR reflects vertical load transfer from the inside to the outside wheels w.r.t the corner (turn). An estimation of LTR is given in (8) as a function of the roll angle and its rate of change Rajamani (2012):

$$LTR = r_1\theta + r_2\dot{\theta}, \tag{8}$$

where r_1 and r_2 are identified depending on the vehicle parameters. LTR varies between -1 and 1. When $|LTR| > \overline{LTR}$, where $\overline{LTR}$ a positive constant higher threshold, a rollover risk is detected. Under a lower positive constant threshold $\underline{LTR}$, the vehicle is not subjected to a rollover risk.

3. Centralized vs decentralized control architectures

3.1. Vehicle-related Architectures Overview

3.1.1. Centralized approach

The global centralized multilayer control architecture is shown in Fig. 2. In the control layer, the controlled variables i.e. the vehicle yaw rate $\dot{\psi}$, the vehicle side-slip angle β, and the suspended mass roll angle θ are fed-back from "SCANeR Studio" vehicle and are controlled/optimized together by the optimal $MIMO\ LPV/\mathscr{H}_\infty$ centralized controller, to simul-

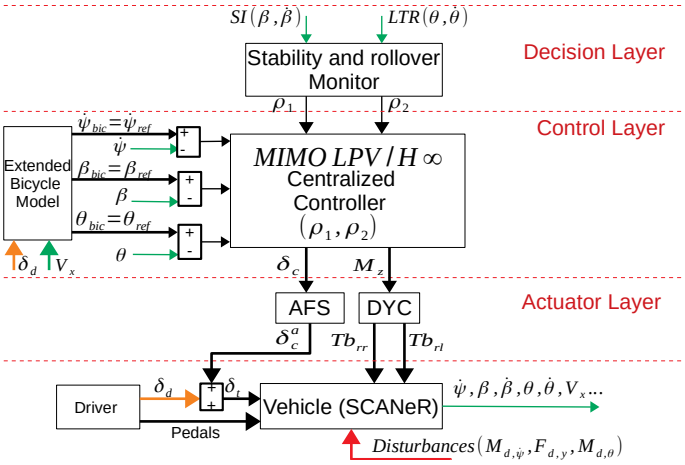

Figure 2.: Centralized global chassis control architecture

taneously enhance the vehicle maneuverability, the lateral stability and the rollover avoidance. Trajectories' references $\dot{\psi}_{ref}$, β_{ref}, and θ_{ref} of the controlled variables are exactly the ones generated by the Extended Bicycle Model. Two endogenous time-varying scheduling gains/parameters ρ_1 and ρ_2 schedule the $MIMO\ LPV/\mathscr{H}_\infty$ controller objectives. A decision maker (in the higher layer) monitors the vehicle situation and instantly sends the values of the scheduling parameters, based on lateral stability (SI) and rollover (LTR) criteria. Based on all these information, the $MIMO\ LPV/\mathscr{H}_\infty$ centralized controller generates the control steering angle δ_c and the corrective yaw moment M_z as the control inputs, while considering actuators constraints (saturation and cut-off frequencies), to maintain the overall closed-loop stability.

3.1.2. Decentralized approach

The global decentralized multilayer control architecture is shown in Fig. 3. The main difference w.r.t the centralized one is in the control layer, where each control input is generated by neglecting the other. Intuitively, AFS control input δ_c is devoted to control the yaw rate $\dot{\psi}$ and the roll angle θ, while DYC control input M_z is privileged to control side-slip angle β, to restrain the braking actuation. Later in the paper, it is proven that each standalone controller is stable by itself, while the overall closed-loop stability problem arises because of the decoupling of control problem. However, this procedure represents a heuristic solution to facilitate the controller development complexity, by benefiting from the robustness of the super-twisting algorithm. For more simplicity, actuators constraints are not considered in the controller structure, while a posterior filter is implemented to make the control inputs feasible. The decision layer is similar in structure to the one of the centralized approach. Based on (SI) and (LTR), it generates three weighting gains $\lambda_{\dot{\psi}}$, λ_β and λ_θ. These gains are reduced to two because, as explained later, λ_β and $\lambda_{\dot{\psi}}$ are linearly dependent variables. The goal of these gains is to promote/attenuate the $STSM$ controllers depending on the driving situation. These gains are introduced into the reference trajectories, by modifying the extended bicycle model trajectories, to maintain each standalone controller stability (more details on the way these gains are injected in the controllers are given later).

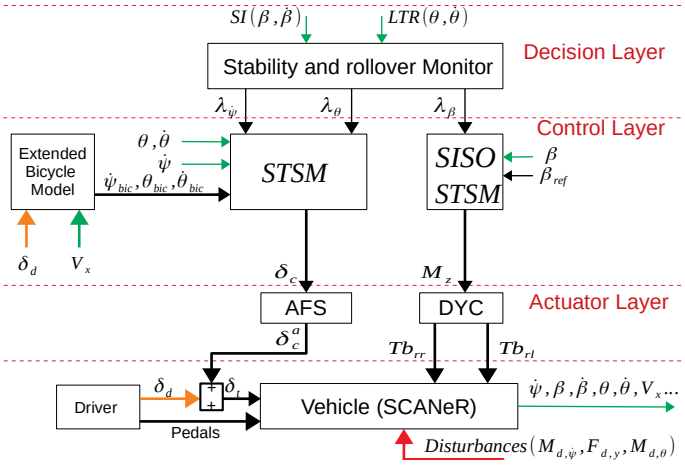

Figure 3.: Decentralized global chassis control architecture

3.1.3. Architectures comparison criteria

A general methodology to compare the centralized and decentralized architectures could contain several criteria like for example design complexity, performance, robustness, scalability, computational time, closed-loop stability, sensors and actuators fault tolerance, failure diagnosability, functional safety, etc... Table 2 provides some general comparison criteria between both control architectures Chen (2016), Rajamani (2012). However, this paper mainly focuses on the design of both centralized and decentralized control architectures, with global performances evaluation and robustness observations with respect to some parameter variations (vehicle speed, road adherence).

3.2. Control layers

In this sub-section, a detailed description of the control layer of both the centralized and decentralized global chassis control architectures is presented.

3.2.1. Centralized control layer synthesis: LPV/$\mathscr{H}_\infty$ controller

The control layer architecture is drawn in Fig. 4. As a standard $\mathscr{H}_\infty$ structure, it contains the controller $K_{LPV/\mathscr{H}_\infty}(\rho_1,\rho_2)$ to be synthesized, and the generalized plant $\sum_g$, where $\rho_1(SI)$ and $\rho_2(LTR)$ are two endogenous weighted parameters calculated by the decision making monitor to adapt the controller dynamics and performances according to the driving conditions. The controller $K_{LPV/\mathscr{H}_\infty}(\rho_1,\rho_2)$ has as inputs the errors between the desired trajectories and the actual ones of the yaw rate $e_{\dot{\psi}}$, the side-slip angle e_β, and the roll angle e_θ. Since the $\mathscr{H}_\infty$ approach is a model-based robust control technique, the actual yaw rate, side-slip angle, and roll angle are calculated based on a LTI vehicle model of (4) (*Plant P*).
Plant P of the generalized plant $\sum_g$ is expressed in (4). It has δ_c and M_z as control inputs; $M_{d,\psi}$, $F_{d,y}$, and $M_{d,\theta}$ as disturbances (exogenous inputs); and the actual yaw rate $\dot{\psi}$, side-slip angle β, and roll angle θ as outputs to be controlled. The remaining subsystems of $\sum_g$ i.e. the weighting functions $W_{\dot{\psi}}(\rho_1)$, $W_\beta(\rho_1)$, $W_\theta(\rho_2)$, $W_\delta(\rho_1,\rho_2)$, and $W_{M_z}(\rho_1)$ of Fig. 4 are defined to characterize the performance objectives Z_1, Z_2, and Z_3 and the actuators' constraints Z_4, and Z_5 (Dynamics of the actuators, given in Subsection 3.4, are neglected during the controller design process). The general form of these weights Doumiati (2014) is given by the following (numerical values are given in Section 3.4, since they depend on the simulated vehicle and

Table 2.: Centralized Vs Decentralized Architectures

Criteria	Centralized	Decentralized
Performance (including robustness)	Very good quality	Good quality
Design Complexity	Complex	Simple
Scalability	Not scalable (Re-design)	scalable (add sub-system)
Computational time	Slow (central calculator)	Quick (several calculators)
Sensors fault effect	Could damage the overall system	Damage only corresponding sub-system
Actuator fault effect	Passive/adaptive fault tolerance possible	Active fault tolerance needed (new configuration)
Closed-loop stability	Global system	Local sub-systems
Failure diagnosability	Complex (complexity of isolating elementary sub-systems with SISO)	Feasible (elementary sub-systems can be monitored and checked)

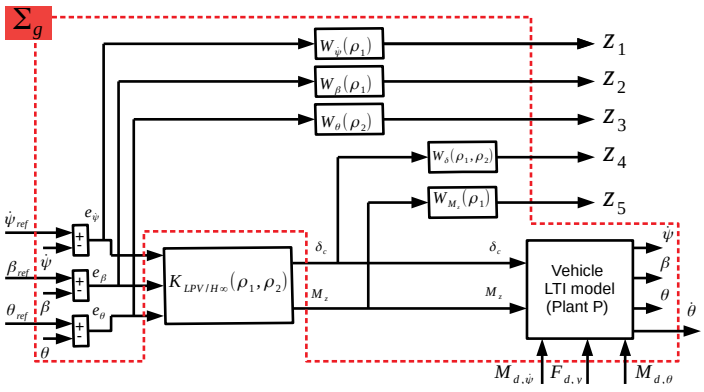

Figure 4.: Control layer architecture

integrated actuators):
- $W_{\dot{\psi}}(\rho_1)$ weights the yaw rate control objective:

$$W_{\dot{\psi}}(\rho_1) = \rho_1 \frac{s/M_1 + 2\pi f_1}{s + 2\pi f_1 A_1}, \tag{9}$$

where M_1 is sufficiently high for a large robustness margin, and A_1 is the tolerated tracking error on $e_{\dot{\psi}}$. $W_{\dot{\psi}}(\rho_1)$ is shaped to reduce the yaw rate error in the range of frequencies below a roll-off frequency f_1 where the vehicle operates Heissing (2010). $W_{\dot{\psi}}(\rho_1)$ is linearly parametrized by the varying parameter ρ_1, where $\rho_1 \in \left\{ \underline{\rho_1} \leq \rho \leq \overline{\rho_1} \right\}$ ($\underline{\rho_1}$ and $\overline{\rho_1}$ are constants representing the lower and higher values of ρ_1). When $\rho_1 = \overline{\rho_1}$, the performance objective $e_{\dot{\psi}}$ is prioritized (maneuverability is enhanced), on the contrary, when $\rho_1 = \underline{\rho_1}$, $e_{\dot{\psi}}$ is relaxed (lateral stability becomes a priority).
- $W_\beta(\rho_1)$ weights the side-slip angle control objective:

$$W_\beta(\rho_1) = \frac{1}{\rho_1} \frac{s/M_2 + 2\pi f_2}{s + 2\pi f_2 A_2}. \tag{10}$$

M_2, A_2 and f_2 have similar meanings as M_1, A_1 and f_1. $W_\beta(\rho_1)$ is designed similarly to $W_{\dot{\psi}}(\rho_1)$. The main difference is that $W_\beta(\rho_1)$ is inversely dependent on the varying parameter ρ_1. This is because the lateral stability is more prioritized than maneuverability in critical situations. This issue is explained later in the decision layer.
- $W_\theta(\rho_2)$ weights the roll angle control objective according to a scheduling parameter ρ_2:

$$W_\theta(\rho_2) = \rho_2 \frac{s/M_3 + 2\pi f_3}{s + 2\pi f_3 A_3}. \tag{11}$$

M_3, A_3 and f_3 have similar meanings as M_1, A_1 and f_1. $W_\theta(\rho_2)$ is linearly parametrized by the varying parameter ρ_2, where $\rho_2 \in \left\{ \underline{\rho_2} \leq \rho_2 \leq \overline{\rho_2} \right\}$ ($\underline{\rho_2}$ and $\overline{\rho_2}$ are constants representing the lower and higher values of ρ_2). When $\rho_2 = \overline{\rho_2}$, the performance objective e_θ is prioritized (rollover avoidance is a priority). On the contrary, when $\rho_2 = \underline{\rho_2}$, e_θ is relaxed (rollover is not a risk).
- $W_\delta(\rho_1, \rho_2)$ weights the steering control input, δ_c:

$$\begin{aligned} W_\delta(\rho_1, \rho_2) &= \left(\frac{1}{\rho_1} + \frac{1}{\rho_2}\right) G_\delta^0 \frac{(s/2\pi f_4 + 1)(s/2\pi f_5 + 1)}{(s/\alpha 2\pi f_5 + 1)^2}, \\ G_\delta^0 &= \frac{(\Delta_f/\alpha 2\pi f_5 + 1)^2}{(\Delta_f/2\pi f_4 + 1)(\Delta_f/2\pi f_5 + 1)}, \\ \Delta_f &= 2\pi(f_4 + f_5)/2, \end{aligned} \tag{12}$$

where $[f_4, f_5]$ is the filter bandwidth. This filter forces the steering system to act at frequencies higher than the driver ones (f_4), to avoid driver annoyance, and lower than the actuator cut-off frequency (f_5). This filter design is inspired from Doumiati (2014). The novelty here is the dependency of $W_\delta(\rho_1, \rho_2)$ on ρ_1 and ρ_2, which allows to relax (promote) or penalize the steering depending on all possible situations. For instance, when rollover stability risk occurs, active steering is relaxed/promoted to maintain vertical stability.

- $W_{M_z}(\rho_1)$ weights the braking control input, M_z:

$$W_{M_z}(\rho_1) \quad = \quad \rho_1 10^{-5} \frac{s/(2\pi f_6)+1}{s/(\kappa 2\pi f_6)+1}, \tag{13}$$

where f_6 is the braking actuator cut-off frequency and κ to handle the braking actuator limitations (see Doumiati (2013)). When $\rho_1 = \overline{\rho_1}$, the braking input is penalized, on the contrary, when $\rho_1 = \underline{\rho_1}$, the braking control signal is relaxed. This design will be related to the vehicle lateral stability.
The controlled outputs Z_1, Z_2, Z_3, Z_4, and Z_5 have to be minimized for any exogenous input. To do so, the powerful $\mathscr{H}_\infty$ control technique is applied here. See Sename (2013) and W. Gu (2005) for more information about the robust $(LPV)\mathscr{H}_\infty$ theory.
Interconnection between $\sum_g$ subsystems is done using "*sysic*" Matlab function (Robust Control Toolbox). Since the generalized plant $\sum_g$ is *LPV* Apkarian (1995), it can be formulated as:

$$\Sigma_g(\rho): \begin{bmatrix} \dot{x} \\ z \\ y \end{bmatrix} = \begin{bmatrix} A(\rho) & B_1(\rho) & B_2(\rho) \\ C_1(\rho) & D_{11}(\rho) & D_{12}(\rho) \\ C_2 & D_{21} & 0 \end{bmatrix} \begin{bmatrix} x \\ w \\ U \end{bmatrix}, \tag{14}$$

where $\rho = \{\rho_1, \rho_2\}$, x includes the state variables of *Plant P* and of the weighting functions, $w = [\dot{\psi}_{ref}, \beta_{ref}, \theta_{ref}, M_{d,\psi}, F_{d,y}, M_{d,\theta}]^T$ is the exogenous input vector, $U = [\delta_c, M_z]^T$ represents the control inputs, $y = [\dot{\psi}, \beta, \theta]^T$ is the measurement vector fed-back to the controller, $y_e = [\dot{\theta}]^T$ is the exogenous output, and $z = [Z_1, Z_2, Z_3, Z_4, Z_5]^T$ is the weighted controlled output vector.
Note that the matrices B_2, and D_{12} depend on ρ, which is not compatible with $\mathscr{H}_\infty$ requirements for polytopic systems. However, this issue is relaxed using some filter on the control input Apkarian (1995).

***Problem resolution:** LMI based LPV/$\mathscr{H}_\infty$:*

The *LPV*/$\mathscr{H}_\infty$ problem consists in finding the controller $K_{LPV/\mathscr{H}_\infty}(\rho_1, \rho_2)$, scheduled by the parameters ρ_1 and ρ_2, such that:

$$K_{LPV/\mathscr{H}_\infty}(\rho): \begin{bmatrix} \dot{x}_c \\ u \end{bmatrix} = \begin{bmatrix} A_c(\rho) & B_c(\rho) \\ C_c(\rho) & 0 \end{bmatrix} \begin{bmatrix} x_c \\ y \end{bmatrix}, \tag{15}$$

which minimizes the $\mathscr{H}_\infty$ norm of the closed-loop *LPV* system formed by the interconnection of equations (14) and (15).
Thanks to the Bounded Real Lemma (BRL) extended to LPV systems, this controller can be found. According to system (14) and via the change of basis expressed in Scherer (1997), a non conservative *LMI* that expresses the same problem as the BRL is formulated in (16) (see next page) and solved by a Semi-Definite Program (SDP), while minimizing γ for $\rho \in \Omega = [\underline{\rho_1}, \overline{\rho_1}] \times [\underline{\rho_2}, \overline{\rho_2}]$. The polytopic approach aims at finding $\widetilde{A}$, $\widetilde{B}$ and $\widetilde{C}$ at each vertex of the polytope described by $\rho \in \Omega$, by using a common Lyapunov function, i.e common $X > 0$ and $Y > 0$. Thus, the solution can be obtained by solving the system (17) at each vertex

$$\begin{bmatrix} A(\rho)X + XA(\rho)^T + B_2\widetilde{C}(\rho) + \widetilde{C}(\rho)^T B_2^T & (*)^T & (*)^T & (*)^T \\ \widetilde{A}(\rho) + A(\rho)^T & YA(\rho) + A(\rho)^T Y + \widetilde{B}(\rho)C_2 + C_2^T \widetilde{B}(\rho)^T & (*)^T & (*)^T \\ B_1(\rho)^T & B_1(\rho)^T Y + D_{21}^T \widetilde{B}(\rho)^T & -\gamma I & (*)^T \\ C_1(\rho)X + D_{12}\widetilde{C}(\rho) & C_1(\rho) & D_{11}(\rho) & -\gamma I \end{bmatrix} < 0; \tag{16}$$

$$\begin{bmatrix} X(\rho) & I \\ I & Y(\rho) \end{bmatrix} > 0.$$

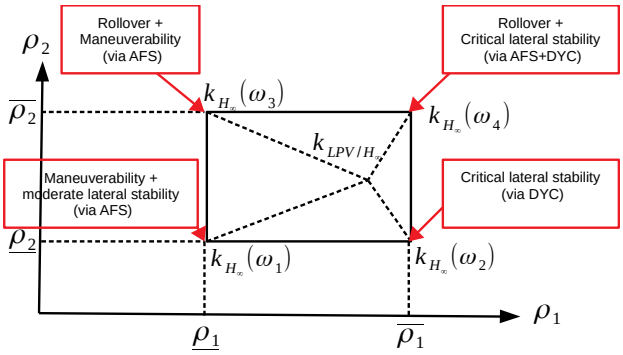

Figure 5.: Controller - Polytopic approach

$\left\{\omega_1 = (\underline{\rho_1}, \underline{\rho_2}), \omega_2 = (\overline{\rho_1}, \underline{\rho_2}), \omega_3 = (\underline{\rho_1}, \overline{\rho_2}), \omega_4 = (\overline{\rho_1}, \overline{\rho_2})\right\}$ of the convex hull Ω:

$$\left\{ \begin{array}{lcl} C_c(\rho) & = & \widetilde{C}(\rho)M^{-T} \\ B_c(\rho) & = & N^{-1}\widetilde{B}(\rho) \\ A_c(\rho) & = & N^{-1}(\widetilde{A}(\rho) - YA(\rho)X - NB_c(\rho)C_2X \\ & - & YB_2(\rho)C_c(\rho)M^{-T})M^{-T} \end{array} \right. , \tag{17}$$

where $M(\rho)$ and $N(\rho)$ are defined by the user so that $M(\rho)N(\rho)^T = I - X(\rho)Y(\rho)$. See Scherer (1997) for more details on the computation solution.
According to the polytopic approach, the final controller, $K_{LPV/\mathscr{H}_\infty}(\rho_1, \rho_2)$, is a convex combination of the controllers synthesized at the vertices of the polytope Apkarian (1995) such as:

$$\begin{aligned} K_{LPV/\mathscr{H}_\infty}(\rho_1, \rho_2) = \alpha_1 K_{\mathscr{H}_\infty}(\omega_1) + \alpha_2 K_{\mathscr{H}_\infty}(\omega_2) \\ + \alpha_3 K_{\mathscr{H}_\infty}(\omega_3) + \alpha_4 K_{\mathscr{H}_\infty}(\omega_4), \end{aligned} \tag{18}$$

where $\sum_{i=1}^{i=4} \alpha_i(\rho_1, \rho_2) = 1$; $\alpha_i(\rho_1, \rho_2) > 0$. The polytopic coordinates $\alpha_i(\rho_1, \rho_2)$ weight the controllers on the vertices to construct the final controller, depending on the driving situation, as shown in Fig. 5. An instant evaluation of $\alpha_i(\rho_1, \rho_2)$ is given by the following equations (the Matlab function"*polydec*" (Robust Control Toolbox) is also useful to evaluate polytopes with more vertices):

$$\begin{aligned} \alpha_1 &= \frac{\overline{\rho_1} - \rho_1}{\overline{\rho_1} - \underline{\rho_1}} \times \frac{\overline{\rho_2} - \rho_2}{\overline{\rho_2} - \underline{\rho_2}}; \quad & \alpha_3 &= \frac{\overline{\rho_1} - \rho_1}{\overline{\rho_1} - \underline{\rho_1}} \times \frac{\rho_2 - \underline{\rho_2}}{\overline{\rho_2} - \underline{\rho_2}}; \\ \alpha_2 &= \frac{\rho_1 - \underline{\rho_1}}{\overline{\rho_1} - \underline{\rho_1}} \times \frac{\overline{\rho_2} - \rho_2}{\overline{\rho_2} - \underline{\rho_2}}; \quad & \alpha_4 &= \frac{\rho_1 - \underline{\rho_1}}{\overline{\rho_1} - \underline{\rho_1}} \times \frac{\rho_2 - \underline{\rho_2}}{\overline{\rho_2} - \underline{\rho_2}}. \end{aligned} \tag{19}$$

$$\dot{X} = \begin{bmatrix} \ddot{\psi} \\ \dot{\beta} \\ \dot{\theta} \\ \ddot{\theta} \end{bmatrix} = \underbrace{\begin{pmatrix} a_{11} & a_{12} & a_{13} & a_{14} \\ a_{21} & a_{22} & a_{23} & a_{24} \\ 0 & 0 & 0 & 1 \\ a_{41} & a_{42} & a_{43} & a_{44} \end{pmatrix}}_{A} \underbrace{\begin{bmatrix} \dot{\psi} \\ \beta \\ \theta \\ \dot{\theta} \end{bmatrix}}_{X} + \underbrace{\begin{pmatrix} b_{u,11} \\ b_{u,21} \\ 0 \\ b_{u,41} \end{pmatrix}}_{B_{u,1}} \underbrace{[\delta_c]}_{U1} + \underbrace{\begin{pmatrix} b_{d,11} & 0 & 0 \\ 0 & b_{d,22} & 0 \\ 0 & 0 & 0 \\ 0 & 0 & b_{d,43} \end{pmatrix}}_{B_d} \underbrace{\begin{bmatrix} M_{d,\psi} \\ F_{d,y} \\ M_{d,\theta} \end{bmatrix}}_{D}; \tag{20}$$

$$y = X.$$

$$\dot{X} = \begin{bmatrix} \ddot{\psi} \\ \dot{\beta} \\ \dot{\theta} \\ \ddot{\theta} \end{bmatrix} = \underbrace{\begin{pmatrix} a_{11} & a_{12} & a_{13} & a_{14} \\ a_{21} & a_{22} & a_{23} & a_{24} \\ 0 & 0 & 0 & 1 \\ a_{41} & a_{42} & a_{43} & a_{44} \end{pmatrix}}_{A} \underbrace{\begin{bmatrix} \dot{\psi} \\ \beta \\ \theta \\ \dot{\theta} \end{bmatrix}}_{X} + \underbrace{\begin{pmatrix} b_{u,12} \\ b_{u,22} \\ 0 \\ b_{u,42} \end{pmatrix}}_{B_{u,2}} \underbrace{[M_z]}_{U2} + \underbrace{\begin{pmatrix} b_{d,11} & 0 & 0 \\ 0 & b_{d,22} & 0 \\ 0 & 0 & 0 \\ 0 & 0 & b_{d,43} \end{pmatrix}}_{B_d} \underbrace{\begin{bmatrix} M_{d,\psi} \\ F_{d,y} \\ M_{d,\theta} \end{bmatrix}}_{D}; \tag{21}$$

$$y = X.$$

3.2.2. Decentralized control layer synthesis: Super-Twisting Sliding Mode STSM controllers

In an intuitive way, the decentralized approach decouples the control problem into two sub-problems: AFS is responsible on the control of the vehicle yaw rate $\dot{\psi}$ and the roll angle θ by neglecting the effect of the DYC on these dynamics when developing the controller; DYC which is effective to control both the vehicle yaw rate and the side-slip angle, is privileged to control only the side-slip angle β to limit its intervention, in order to prevent long braking durations which decelerate the vehicle, annoy the driver and cause long term tires wearing. To be noted also, as a consequence of the AFS controller, the side-slip angle is enhanced in the low-to-mid range of lateral stability, while it becomes ineffective at high critical lateral dynamics.

The *STSM* AFS control synthesis model (20) is similar to (4), while considering $M_z = 0$, and thus, reducing B_u to its first column. The driver steering input δ_d is neglected in the synthesis model, and then it is considered as a feed-forward of the entire system.

The *STSM* DYC control synthesis model (21) is similar to (4), while considering $\delta_c = 0$, and thus, reducing B_u to its second column. The driver steering input δ_d is also neglected in the synthesis model, and then it is considered as a feed-forward of the entire system.

Under these assumptions, a robust control technique, which deals with modeling uncertainties and decoupling phenomenon, is needed. Thus, the super-twisting sliding mode *STSM* control technique, which is one of the most powerful robust control techniques that suit this control problem is chosen.

The super-Twisting algorithm is a second order sliding mode control that handles a relative degree equal to one. It generates the continuous control function that drives the sliding variable and its derivative to zero in finite time in the presence of smooth matched disturbances.

Consider the affine system form written as:

$$\ddot{X} = f(X,t) + g(X,t)u(t), \tag{22}$$

where $X = [\dot{\psi}, \beta, \theta, \dot{\theta}]^T$, and $f(X,t) = AX$. In the case of the AFS controller synthesis $g(X,t) = B_{u,1}$ and $u = \delta_c$ as can be seen from (20). In the case of the DYC controller synthesis $g(X,t) = B_{u,2}$ and $u = M_z$ as can be seen from (21).

Let define $E = [e_{\dot{\psi}}, e_\beta, e_\theta, \dot{e}_\theta]^T = [\dot{\psi} - \dot{\psi}_{ref}, \beta - \beta_{ref}, \theta - \theta_{ref}, \dot{\theta} - \dot{\theta}_{ref}]^T$ the error vector between the actual and the desired states. $\dot{\psi}_{ref}$, β_{ref}, θ_{ref}, and $\dot{\theta}_{ref}$ depend on the extended bicycle model and the weighting gains sent from the decision layer. Their expressions are given later in this section.

Let define three sliding variables as the following:

$$\begin{aligned} s_{\dot{\psi}} &= e_{\dot{\psi}} = \dot{\psi} - \dot{\psi}_{ref}, \\ s_{\beta} &= e_{\beta} = \beta - \beta_{ref}, \\ s_{\theta} &= \dot{e}_{\theta} + k_{\theta}\, e_{\theta} = (\dot{\theta} - \dot{\theta}_{ref}) + k_{\theta}(\theta - \theta_{ref}), \end{aligned} \tag{23}$$

where $s_{\dot{\psi}}$ (resp. s_{θ}) has a relative degree of 1 w.r.t the control input δ_c since $b_{u,11}$ (resp. $b_{u,41}$) is not zero as can be seen in the AFS synthesis model of (20). Similarly, s_{β} has a relative degree of 1 w.r.t the control input M_z since $b_{u,11}$ is not zero as can be seen in the DYC synthesis model of (21). k_{θ} is a positive constant gain which determines the time convergence of the state errors $\dot{e}_{\theta}$ and e_{θ}.
Since the AFS is responsible of the control of both state variables $\dot{\psi}$ and θ, let define a new sliding variable $s_{\dot{\psi},\theta}$ such that:

$$s_{\dot{\psi},\theta} = c_1 s_{\dot{\psi}} + c_2 s_{\theta}, \tag{24}$$

where c_1 and c_2 are positive constant weights relatively scaling the sliding variables $s_{\dot{\psi}}$ and s_{θ}.
$s_{\dot{\psi},\theta}$, and s_{β} to be controlled respectively by the AFS and the DYC, have their control inputs appear in their first derivatives (relative degree 1). This means their second derivative can be written as:

$$\ddot{s}(s,t) = \Phi(s,t) + \xi(s,t)\dot{u}(t) \tag{25}$$

where $\Phi(s,t)$ and $\xi(s,t)$ are unknown bounded signals.
The control objective is to achieve the convergence to the sliding surface defined by $s = 0$. Only the knowledge of s is required in real time.
Suppose that there exist positive constants S_0, b_{min}, b_{max}, C_0, U_{max} such that $\forall x \in \Re^n$ and $|s(x,t)| < S_0$, the system satisfies the following conditions:

$$\begin{cases} |u(t)| \leq U_{max} \\ |\Phi(s,t)| < C_0 \\ 0 < b_{min} \leq |\xi(s,t)| \leq b_{max} \end{cases} \tag{26}$$

The sliding mode control law, based on the Super-Twisting algorithm, is given by:

$$u(t) = u_1 + u_2 \begin{cases} u_1 = -\alpha_1 |s|^{\tau} \text{sign}(s), \;\; \tau \in]0,\, 0.5] \\ \dot{u}_2 = -\alpha_2 \text{sign}(s), \end{cases} \tag{27}$$

where α_1 and α_2 are positive gains. The finite time convergence is guaranteed by the following conditions:

$$\begin{cases} \alpha_1 \geq \sqrt{\frac{4C_0(b_{max}\alpha_2 + C_0)}{b_{min}^2(b_{min}\alpha_2 - C_0)}} \\ \alpha_2 > \frac{C_0}{b_{min}} \end{cases} \tag{28}$$

The convergence analysis is shown in Utkin (2013). The function *sign* is smoothed by the approximation $sign(s) = \frac{s}{|s|+\varepsilon}$, where ε is a positive small value.

Based on the above discussion, the STSM control inputs of the AFS and the DYC are respectively given by:

$$\begin{array}{l} \delta_c = -\alpha_{\delta,1}|s_{\psi,\theta}|^{\tau_\delta} sign(s_{\psi,\theta}) - \alpha_{\delta,2}\int_0^t sign(s_{\psi,\theta})d\tau, \\ M_z = -\alpha_{M_z,1}|s_\beta|^{\tau_{M_z}} sign(s_\beta) - \alpha_{M_z,2}\int_0^t sign(s_\beta)d\tau, \end{array} \tag{29}$$

where $\alpha_{\delta,1}$ and $\alpha_{\delta,2}$ (resp. $\alpha_{M_z,1}$ and $\alpha_{M_z,2}$) are positive gains satisfying conditions of (28). τ_δ and τ_{M_z} are constants in the interval $]0, 0.5]$.
The STSM control inputs guarantee the convergence of $s_{\psi,\theta}$ and s_β in a finite time to zero. Once $s_\beta = 0$, this means that the state β is converged to β_{ref}. Once $s_{\psi,\theta} = 0$, this means that $s_\psi = 0$ and $s_\theta = 0$ because the state matrix A is Hurwitz (all eigenvalues in the left half plane). Thus, ψ converges to ψ_{ref} and $\dot{e}_\theta + k_\theta\ e_\theta \to 0$, which means that θ (resp. $\dot{\theta}$) exponentially converges to θ_{ref} (resp. $\dot{\theta}_{ref}$) if $k_\theta > 0$.
As mentioned before, ψ_{ref}, β_{ref}, θ_{ref}, and $\dot{\theta}_{ref}$ depend on the extended bicycle model and the weighting gains sent from the decision layer. Thus, let define

$$\begin{array}{l} \psi_{ref} = \lambda_\psi\ \psi_{bic} + (1-\lambda_\psi)\ \psi, \\ \beta_{ref} = \lambda_\beta \beta_{bic} + (1-\lambda_\beta)\beta, \\ \theta_{ref} = \lambda_\theta \theta_{bic} + (1-\lambda_\theta)\theta, \\ \dot{\theta}_{ref} = \lambda_\theta \dot{\theta}_{bic} + (1-\lambda_\theta)\dot{\theta}, \end{array} \tag{30}$$

where $\lambda_\psi(SI)$, $\lambda_\beta(SI)$ and $\lambda_\theta(LTR)$ are the scheduling gains which vary between 0 and 1. Their instant values are sent from the decision layer depending on the vehicle situation. When one of these gains approaches to 1, this means that the corresponding reference trajectory is equal to the one of the extended bicycle model, thus, the corresponding controller is promoted to control the corresponding variable. When it approaches to 0, this means that the reference trajectory is equal to the actual vehicle one, thus, the control of the corresponding variable is attenuated since the corresponding sliding variable is vanished.
Consequently, the sliding variables of (23) become equivalent to:

$$\begin{array}{l} s_\psi = \dot{\psi} - \dot{\psi}_{ref} = \lambda_\psi\ (\dot{\psi} - \dot{\psi}_{bic}), \\ s_\beta = \beta - \beta_{ref} = \lambda_\beta(\beta - \beta_{bic}), \\ s_\theta = (\dot{\theta} - \dot{\theta}_{ref}) + k_\theta(\theta - \theta_{ref}) = \lambda_\theta[(\dot{\theta} - \dot{\theta}_{bic}) + k_\theta(\theta - \theta_{bic})], \end{array} \tag{31}$$

These new forms of sliding variables mean that the actual state variables are forced to converge to the extended bicycle reference model only if the scheduling gains are high (close to 1). In this case, we say that the control objective is promoted. Otherwise, the control objective is attenuated (relaxed) and the state variables remain without control.
Note: The modification of the sliding variables by the multiplication with the scheduling gains maintains the closed-loop stability of the individual AFS and DYC since these gains are introduced in the reference trajectories.

3.3. Decision Layers

3.3.1. Centralized approach: ρ_1 and ρ_2 calculations

Once the control layer is developed, the decision layer is responsible to monitor the driving situations.

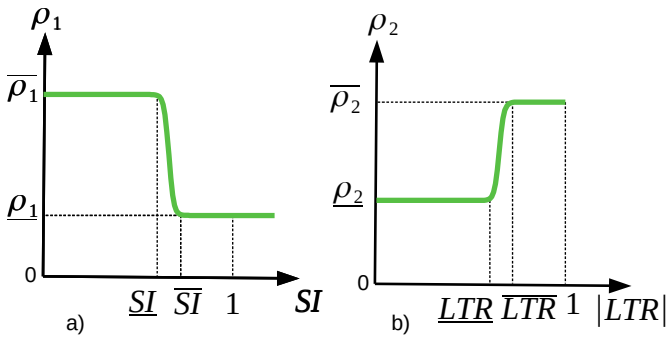

Figure 6.: Scheduling parameters

For $SI \leq \underline{SI}$, the vehicle is in normal driving situations, thus, the AFS is promoted for maneuverability purpose. It also enhances the lateral stability up to a moderate level. In this range, DYC is penalized. When the vehicle reaches critical lateral stability $SI \geq \overline{SI}$, then the DYC is promoted to enhance the lateral stability. Based on this analysis, the scheduled gain ρ_1 is designed to feed the $LPV/\mathscr{H}_\infty$ controller sufficient knowledge about the weights to be promoted or attenuated. A "*sigmoid*" function (32) (see Fig. 6.a) governs the relation between ρ_1 and SI, to ensure a continuous and a relatively smooth variation of ρ_1.

$$\rho_1 = \overline{\rho_1} - \frac{\overline{\rho_1} - \underline{\rho_1}}{1 + e^{-\frac{8}{\overline{SI} - \underline{SI}}(SI - \frac{\overline{SI} + \underline{SI}}{2})}}. \tag{32}$$

When $|LTR| > \overline{LTR}$, where $\overline{LTR}$ a positive constant threshold, a rollover risk is detected, and thus, the controller is informed by the scheduling parameter ρ_2, to handle this risk. To ensure a smooth transition of ρ_2, a lower positive constant threshold $\underline{LTR}$ is defined. A "*sigmoid*" function (33) (see Fig. 6.b) governs the relation between ρ_2 and $|LTR|$.

$$\rho_2 = \underline{\rho_2} + \frac{\overline{\rho_2} - \underline{\rho_2}}{1 + e^{-\frac{8}{\overline{LTR} - \underline{LTR}}(|LTR| - \frac{\overline{LTR} + \underline{LTR}}{2})}}. \tag{33}$$

3.3.2. Decentralized approach: λ_ψ, λ_β and λ_θ calculations

Similar to the decision layer of the centralized approach, the decision layer of the decentralized approach monitors all the control objectives based on monitoring criteria (SI and LTR), then, it calculates and sends instantly the values of λ_ψ, λ_β and λ_θ to attenuate/promote the corresponding control objective depending on the vehicle situation.
λ_ψ approaches to 1 when the vehicle maneuverability is the control objective. This means when $SI \leq \underline{SI}$. In this case, λ_β approaches to 0 since no lateral stability risk is detected. When $SI \geq \overline{SI}$, λ_ψ approaches to 0 because the vehicle maneuverability is not a priority, while λ_β approaches to 1 since the lateral stability risk is high. A "*sigmoid*" function (34) (Fig. 7.a) governs the relation between λ_ψ (resp. λ_β) and SI, to ensure a continuous and a relatively smooth variation of λ_ψ and λ_β.

$$\begin{aligned} \lambda_\beta &= \frac{1}{1 + e^{-\frac{8}{\overline{SI} - \underline{SI}}(SI - \frac{\overline{SI} + \underline{SI}}{2})}}, \\ \lambda_\psi &= 1 - \lambda_\beta. \end{aligned} \tag{34}$$

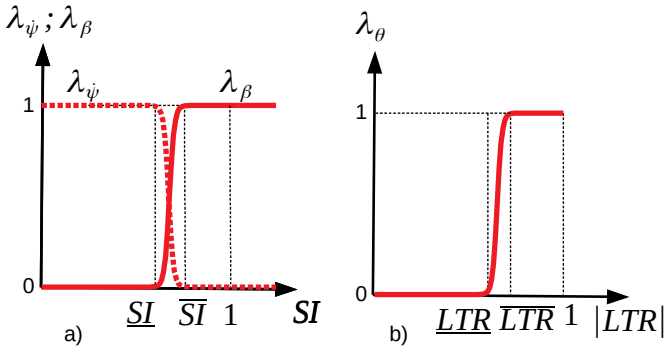

Figure 7.: Scheduling gains λ_ψ and λ_β

By the same reasoning λ_θ is related to LTR. λ_θ approaches to 0 when no rollover risk is detected ($LTR \leq \underline{LTR}$) and approaches to 1 when rollover risk is detected ($LTR \geq \overline{LTR}$). A "*sigmoid*" function (35) (Fig. 7.b) governs the relation between λ_θ and LTR, to ensure a continuous and a relatively smooth variation of λ_θ.

$$\lambda_\theta = \frac{1}{1+e^{-\frac{8}{\overline{LTR}-\underline{LTR}}(LTR-\frac{\overline{LTR}+\underline{LTR}}{2})}}, \tag{35}$$

3.4. Actuator layer

In the actuator layer, the Active Front Steering AFS system is formed by an electrical motor that generates the physical additive steering called "actuator control steering" δ_c^a that tracks δ_c. AFS provides also the mechanical link between δ_c^a and δ_d, the driver steering angle, where the total steering $\delta_t = \delta_c^a + \delta_d$ (for more information refer to Klier (2004)).
In order to ensure that controller demand is achievable by the actuator, a simple actuator model is implemented into the control loop of the actuator layer. AFS actuator is modeled as:

$$\dot{\delta}_c^a = 2\pi f_5(\delta_c - \delta_c^a), \tag{36}$$

where f_5 is the actuator cut-off frequency. This actuator is bounded between $\left[-\delta_{c,max}^a, +\delta_{c,max}^a\right]$, where $\delta_{c,max}^a$ is the saturation of the AFS actuator.
In order to prevent direct interference with the active steering on the front tires, the corrective yaw moment M_z is allocated by the DYC to rear Electro-Mechanical Brakes EMB (right Tb_{rr} and left Tb_{rl}) Doumiati (2013). The DYC moment M_z is generated as a braking torque $T_{b,rj} = \frac{2r}{t_r} M_z$ at one of the rear wheels of radius r (at the same instant), depending on the direction of M_z Doumiati (2014).
The Electro Mechanical Braking (EMB) actuators providing $T_{b,rj}^a$ (that tracks $T_{b,rj}$) model is given by:

$$\dot{T}_{b,rj}^a = 2\pi f_6(T_{b,rj} - T_{b,rj}^a), \tag{37}$$

where f_6 is the actuator cut-off frequency. This actuator control is bounded between $[0, T_{b,max}^a]$, where $T_{b,max}^a$ is the saturation of the EMB actuators.

4. Simulation-based testing

This section is dedicated to test the proposed controllers. Testing is done on "SCANeR studio" simulator, by analyzing several vehicle variables in two scenarios: a double lane change test and a fishhook test; both at an initial speed 110 km/h. Both scenarios are considered as hard tests which solicit the vehicle lateral stability, yet the fishhook test influences more the rollover risk phenomenon since a long duration constant high steering amplitude is applied on the vehicle.
In both scenarios, the comparison is done between an uncontrolled vehicle, where the controller is not implemented ("OL" as Open Loop), and by integrating the proposed controllers i.e. the centralized controller ("$LPV/\mathscr{H}_\infty$") and the decentralized controller ("SM" as Sliding Mode) into the vehicle. Several simulation tests for different scenarios have been done to select the best controller gains for both architectures. Chosen numerical values are provided in Table 3.

4.1. Double lane change scenario

In the double lane change test, the driver is intended to change the lane then go back to the same lane in a short duration. At high speed the vehicle is subjected to lateral stability risk. This simulated test shows the advantage of having such ADAS systems implemented into the vehicle. The driver steering angle applied on the vehicle is represented by the variable δ_d on Fig. 13. The remaining curves of the same figure are discussed later. The proposed control architectures monitor the vehicle situation and control its dynamics to follow, when necessary, the reference trajectories of the extended bicycle model in order to enhance the vehicle maneuverability, lateral stability and rollover avoidance. Figures 8, 9, and 10 respectively show the yaw rate, the side-slip angle and the roll angle which are the controlled variables. Both control architectures (centralized and decentralized) have achieved a high accuracy of tracking the yaw rate and the side-slip angle references, compared to the uncontrolled vehicle. Meanwhile, the roll angle has tracked its reference only in some regions (especially around 1 s and 3 s). These tracking results can be further explained by observing the monitoring criteria (SI and LTR) and the scheduling gains of each architecture. Therefrom, Fig. 11 and Fig. 12 respectively show the lateral stability index and the load transfer ratio with their corresponding scheduling gains of both control architectures. The lateral stability index SI of the uncontrolled vehicles (Fig. 11) exceeds $SI = 1$, which means that the vehicle has lost its stability, while both control architectures have covered back the SI under $SI = \underline{SI}$, and thus, they have succeeded to remain the vehicle stable on almost all the time. When $SI \leq \underline{SI}$ (almost all the time except around 1 s and 3 s), the scheduling gain ρ_1 (resp. $\lambda_{\dot{\psi}}$) of the centralized (resp. decentralized) architecture is set to $\rho_1 = \overline{\rho_1}$ (resp. $\lambda_{\dot{\psi}} = 1$) which accounts for the maneuver-

Table 3.: Controllers' Parameters for Simulation

Parameters	Values
$M_1 = M_2 = M_3; A_1 = A_2 = A_3; \kappa$	$2; 0.1 = 10\%; 100$
$f_1 = f_2 = f_3; f_4; f_5; f_6$	$11.15\ Hz; 1\ Hz; 10\ Hz; 10\ Hz$
$c_1; c_2; k_\theta$	1;1;1
$\alpha_{\delta,1}; \tau_\delta; \alpha_{\delta,2}$	0.5;0.5;0.01
$\alpha_{M_z,1}; \tau_{M_z}; \alpha_{M_z,2}$	500;0.5;0.1
$\underline{\rho_1}; \overline{\rho_1}; \underline{\rho_2}; \overline{\rho_2}$	70;85;75;85
$q_1; q_2; r_1; r_2$	9.55;2.49;12;1
$\underline{SI}; \overline{SI}; \underline{LTR}; \overline{LTR}$	0.6;0.7;0.6;0.7
$\delta^a_{c,max}; T^a_{b,max}$	$5^\circ; 1200\ N.m$

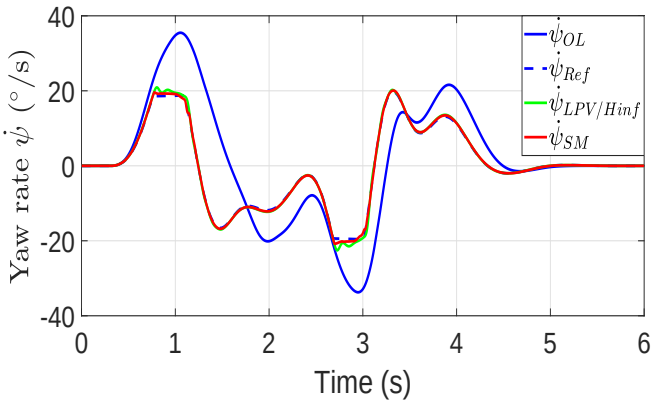

Figure 8.: Yaw rate comparison

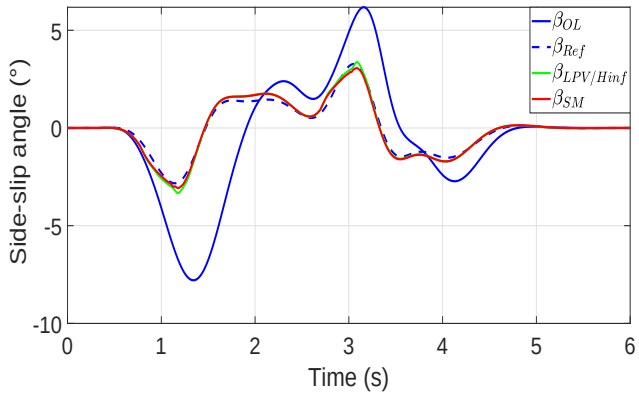

Figure 9.: Side-slip angle comparison

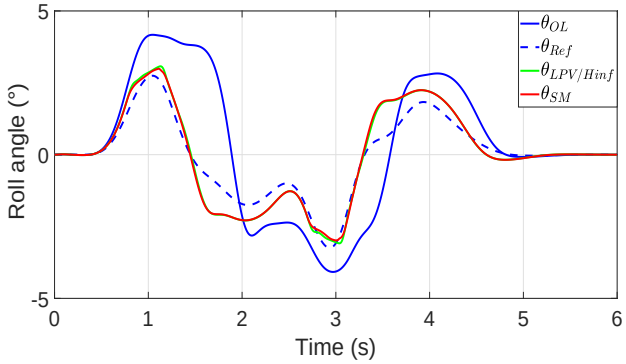

Figure 10.: Roll angle comparison

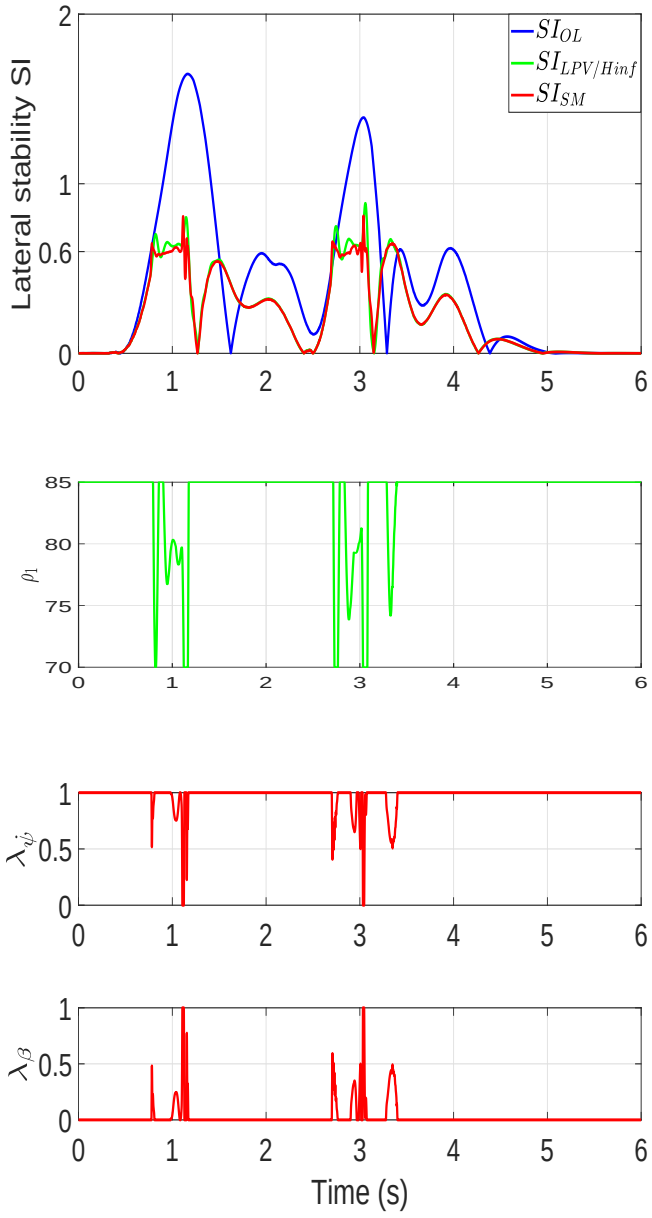

Figure 11.: Lateral stability and scheduling gains

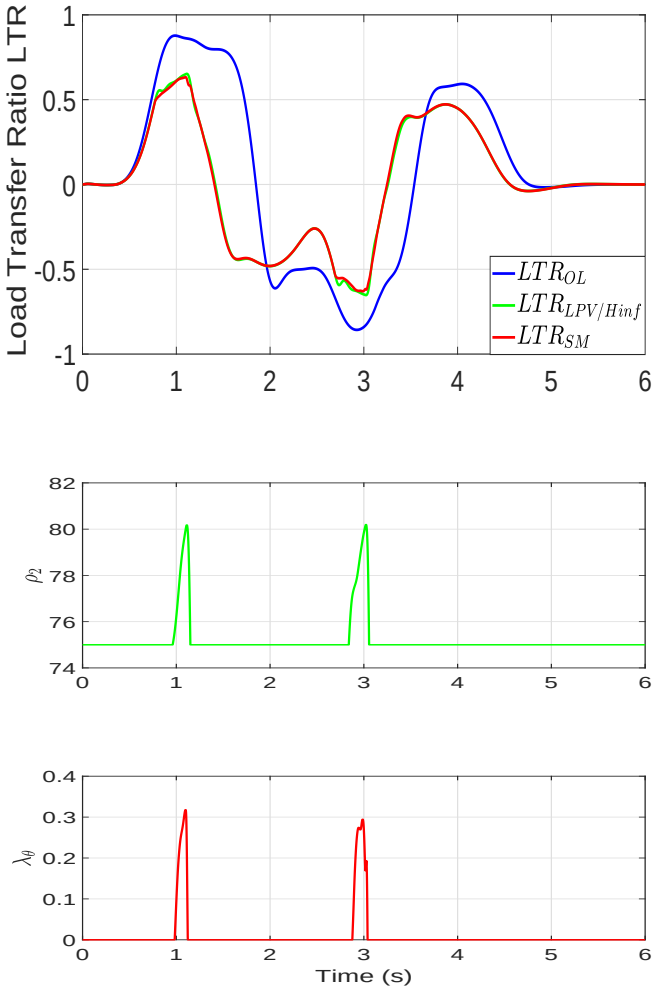

Figure 12.: Load transfer ratio and scheduling gains

ability objective. When $SI \leq \overline{SI}$ (specifically around 1 s and 3 s), the scheduling gain ρ_1 (resp. λ_ψ) of the centralized (resp. decentralized) architecture deviates toward $\rho_1 = \underline{\rho_1}$ (resp. $\lambda_\psi = 0$ or $\lambda_\beta = 1$) which accounts for the lateral stability objective. Based on this discussion, one can conclude on the yaw rate tracking of Fig. 8 almost all the time except around 1 s and 3 s, and on the side-slip angle tracking of Fig. 9 only around 1 s and 3 s. However, the side-slip angle tracks its reference all the time as a consequence of the yaw rate tracking, since both dynamics are correlated, and so their references. The load transfer ratio of the uncontrolled vehicle (Fig. 12) exceeds $LTR = \overline{LTR}$, which means that the vehicle is risky to roll-over, while both control architectures have covered back the LTR under $LTR = \underline{LTR}$ almost all the time except around 1 s and 3 s, and thus, they have succeeded to remove the rollover risk. The scheduling gain ρ_2 (resp. λ_θ) of the centralized (resp. decentralized) architecture was $\rho_2 = \underline{\rho_2}$ (resp. $\lambda_\theta = 0$) almost all the time except around 1 s and 3 s where it deviates to a higher value. This means, only around 1 s and 3 s the proposed control architectures have switched the control objective to rollover avoidance, while at the remaining time of the simulation the LTR is enhanced because the roll angle of Fig. 10 is diminished compared to the uncontrolled one as a consequence of the yaw rate enhancement since both dynamics are correlated. Fig. 13

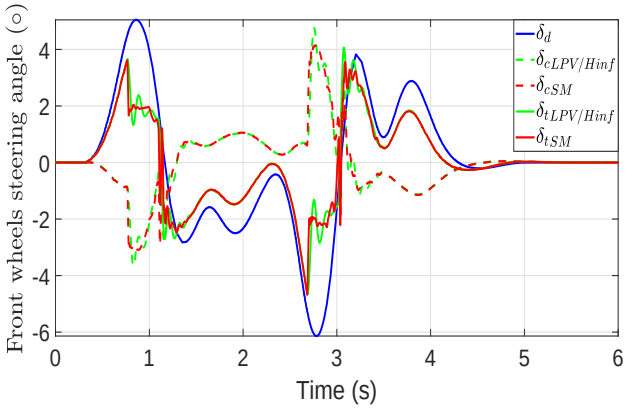

Figure 13.: Steering angle comparison

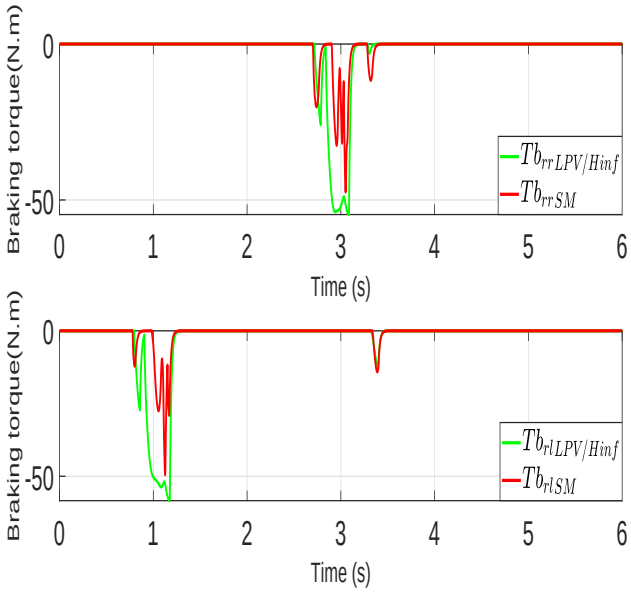

Figure 14.: Braking comparison

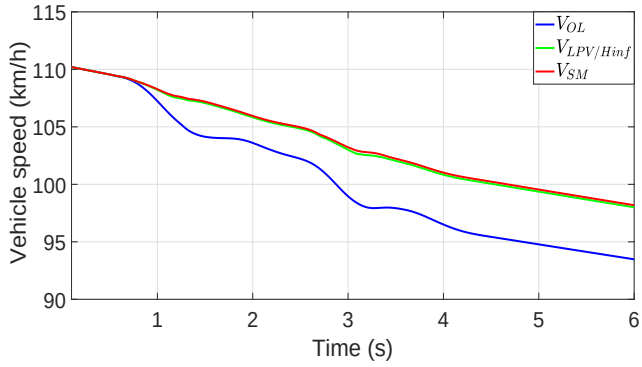

Figure 15.: Vehicle speed comparison

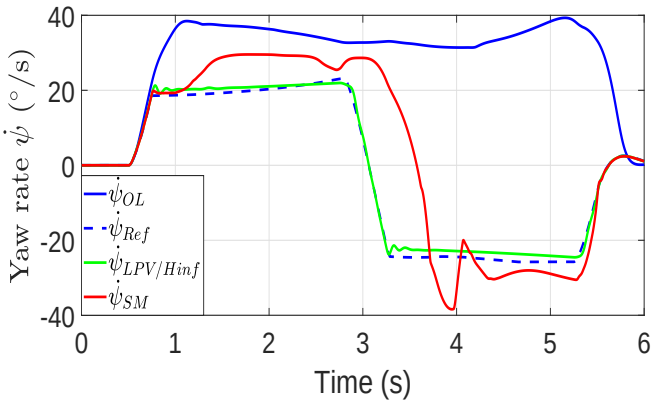

Figure 16.: Yaw rate comparison

shows the driver steering angle δ_d, the AFS steering angle of both controllers δ_c, and the total steering δ_t. One can notice, that both controllers provide similar steering control angles. Fig. 14 shows the braking of the EMB at the left and right rear wheels. The centralized controller activates a little bit more the braking since it is somehow useful to control the roll motion and the yaw rate, on contrary to the decentralized controller which activates the braking only to control the side-slip angle when necessary. The vehicle speed, which drops due to frictions, is improved by both controllers compared to the uncontrolled vehicle since less lost in the lateral motion is achieved as shown in Fig. 15.

4.2. Fishhook scenario

The fishhook test at high speed is a hard test used to perform extremely critical behaviors. It solicits both the lateral stability and the rollover more than in the double lane change. The test consists of turning the steering angle to one direction, keeping a high steer constant angle, then doing the same in the opposite direction. The driver steering angle is shown in Fig. 21. The uncontrolled vehicle yaw rate of Fig. 16 shows that the vehicle turns in one side, and thus, it could not well perform the scenario as the ideal motion should be (reference vehicle). Only the vehicle implemented with the centralized controller could achieve an accurate yaw rate, while the decentralized controller was able to improve the motion without high accuracy. Similar results can be observed on the side-slip angle and the roll angle respectively in Fig. 17 and

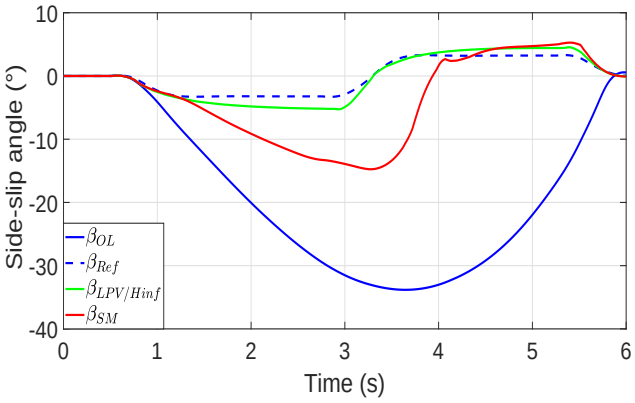

Figure 17.: Side-slip angle comparison

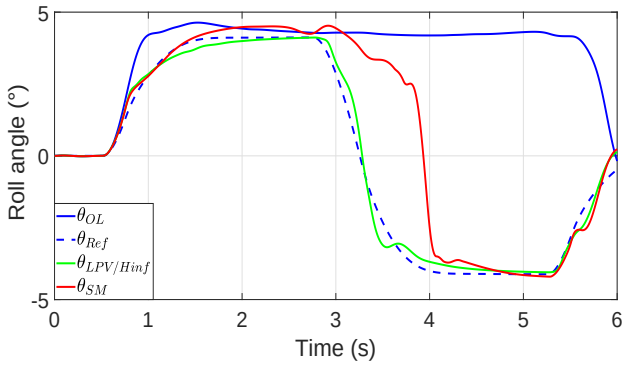

Figure 18.: Roll angle comparison

Fig. 18. Fig. 19 and Fig. 20 respectively show the SI and the LTR with their corresponding scheduling gains. These figures show that the extreme behavior of the uncontrolled vehicle could be reduced but remain unstable using the decentralized controller, while the centralized controller enhances more these behavior providing a marginal stability (the lateral stability and rollover avoidance are achieved but still risky). The fluctuations of the scheduling gains show that this time the controllers are more solicited to ensure the rollover avoidance objective in the presence of the lateral stability risk. The optimality of the centralized solution was more aware about these coupled dynamics which is reflected by the AFS steering angle as can be seen from Fig. 21, where the centralized steering angle was more stable than the decentralized one.

Fig. 22 shows the braking of the EMB at the left and right rear wheels. The centralized controller less activates the braking with an overall enhancement of the root mean square by 48% at the left braking, and 38% at the right braking. The peak amount of the braking is also reduced by 33% at the left wheel, and 14% at the right wheel. The vehicle speed is less dropped in the centralized approach since less braking is applied as can be seen from Fig. 23.

4.3. Simulation-based robustness evaluation

In order to evaluate the robustness of the proposed control architectures with respect to the vehicle speed and road conditions variations, the double lane change test used in Section 4.1

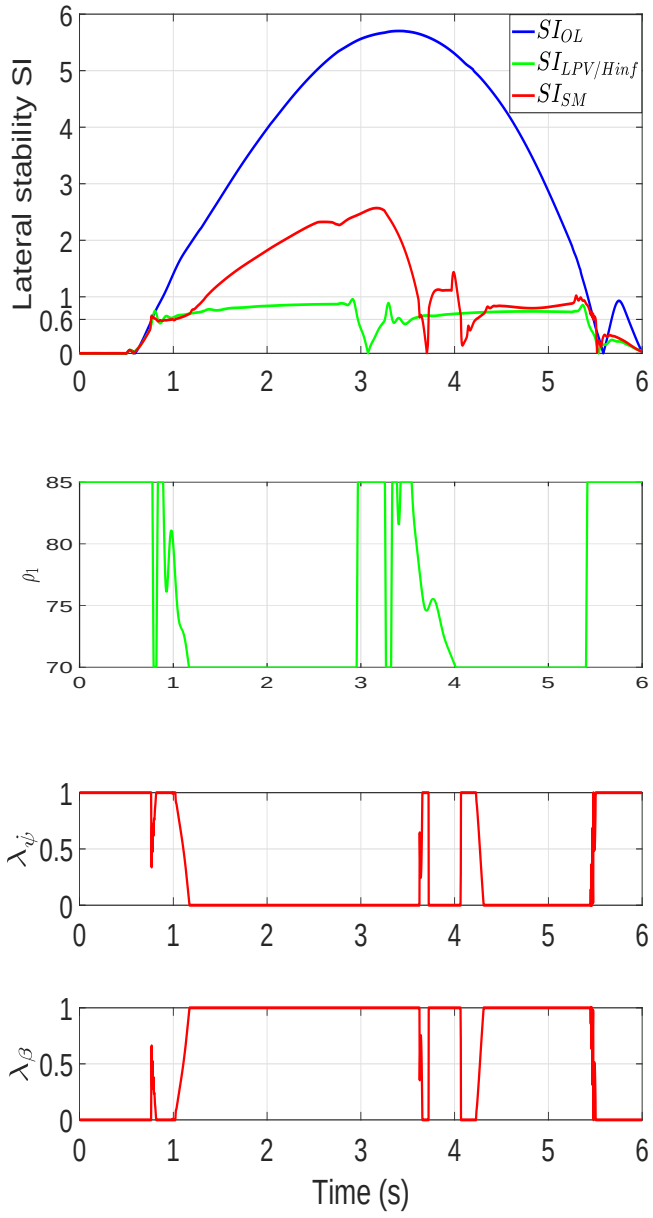

Figure 19.: Lateral stability and scheduled gains

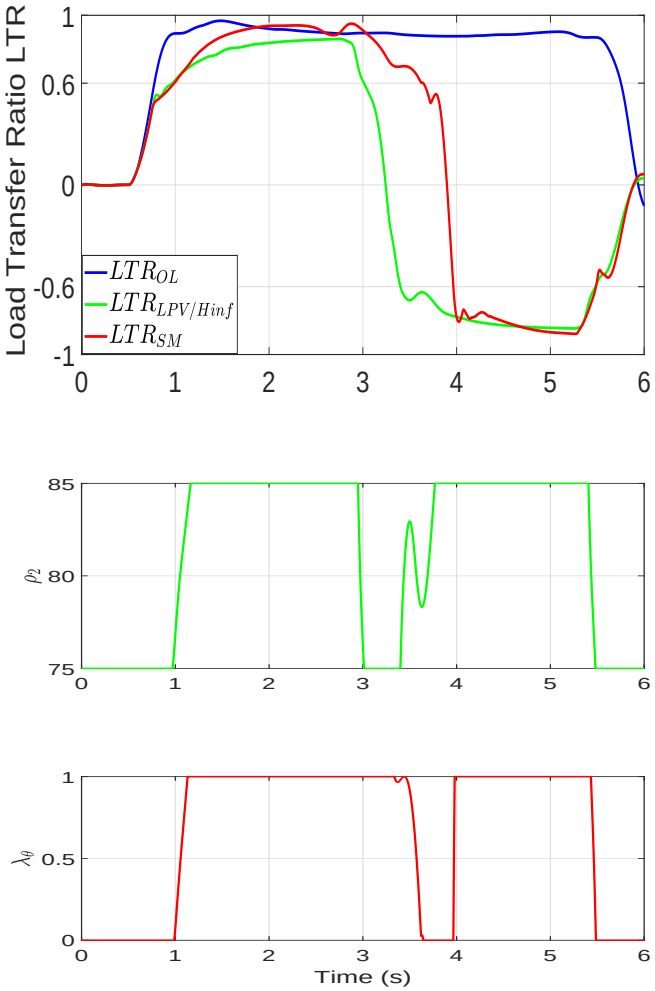

Figure 20.: Load transfer ratio and scheduled gains

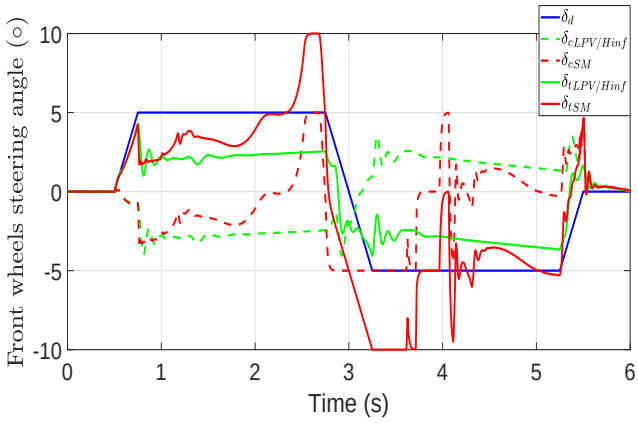

Figure 21.: Steering angle comparison

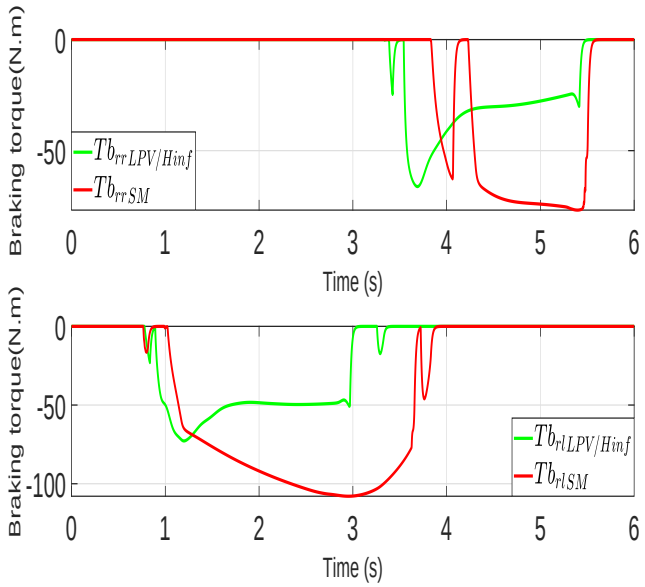

Figure 22.: Braking comparison

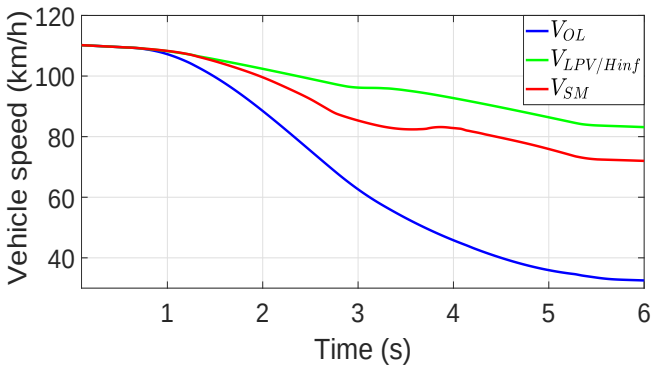

Figure 23.: Vehicle speed comparison

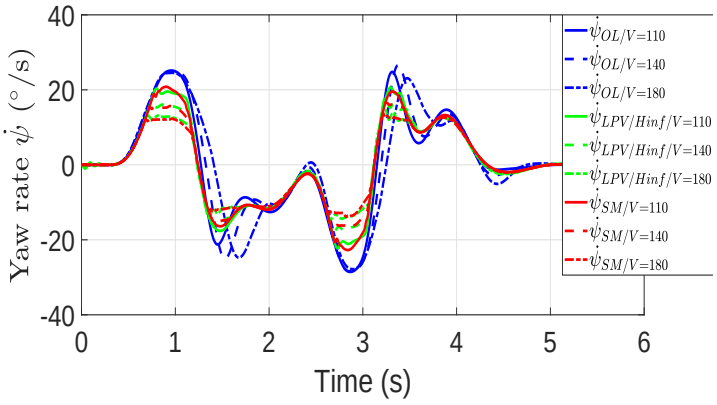

Figure 24.: Robustness to speed variation – Yaw rate comparison

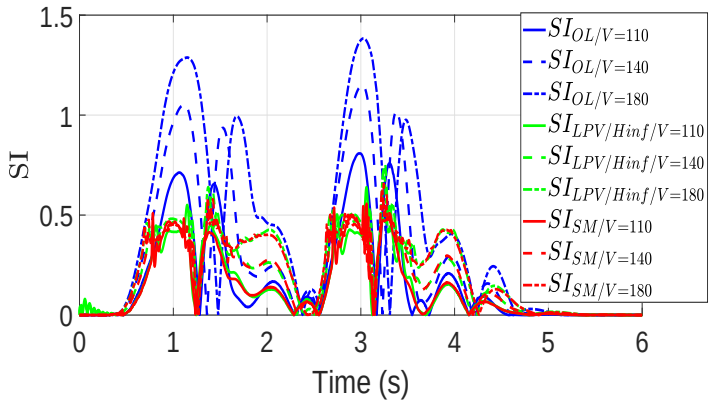

Figure 25.: Robustness to speed variation – Stability Index comparison

is conducted here at different vehicle speeds and under different road conditions.
Figure 24 shows the vehicle yaw rate of the uncontrolled vehicle and both control architectures under three different speeds ($V = 110; 140; 180\ km/h$), where the adherence coefficient is $\mu = 1$. This figure shows that both control architectures are robust to the speed variation, since the vehicle yaw rate is remained lower than the uncontrolled vehicle. Furthermore, both architectures have almost identical properties in terms of speed variation robustness since curves are almost superposed. This observation is confirmed by Figure 25, where both architectures maintain the vehicle stability at the different speeds.
Figure 26 shows the vehicle yaw rate of the uncontrolled vehicle and both control architectures under three different adherence coefficients ($\mu = 1; 0.8; 0.5$), where the vehicle speed is $V = 110 km/h$. This figure shows that both control architectures are robust to a mid-range variation of the adherence coefficient (from $\mu = 1$ to $\mu = 0.8$). However, for a low adherence coefficient ($\mu = 0.5$), only the centralized architecture has succeeded to remain the vehicle under control. This observation is confirmed by Figure 27, where only the centralized architecture has succeeded to maintain the vehicle stability at a low adherence coefficient.

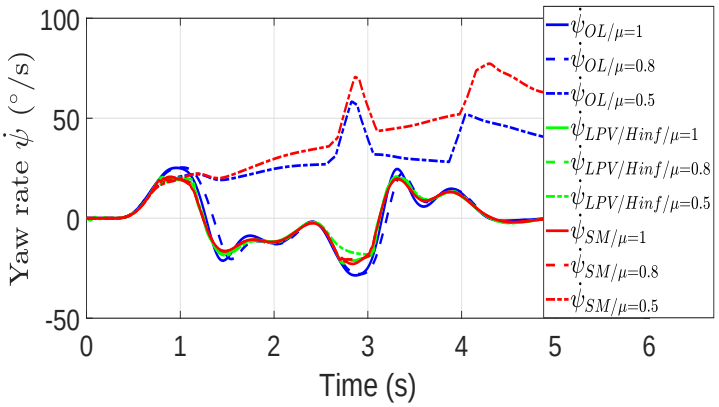

Figure 26.: Robustness to adherence (μ) variation − Yaw rate comparison

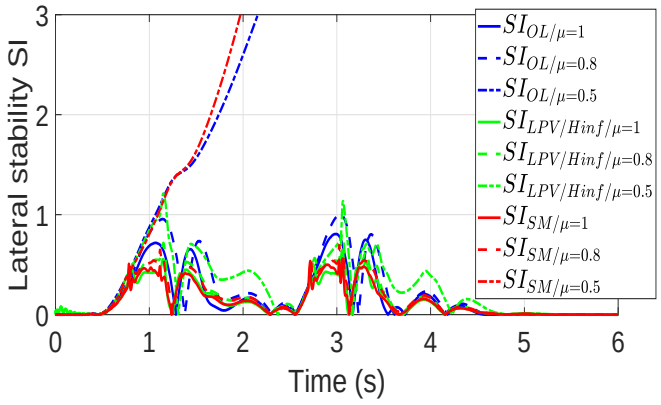

Figure 27.: Robustness to adherence (μ) variation − Stability Index comparison

5. CONCLUSION AND PERSPECTIVES

In this paper, decision-based centralized and decentralized global chassis control architectures have been developed to improve the vehicle maneuverability, the lateral stability and the rollover prevention, by acting on the active front steering and the differential braking. The effectiveness of the proposed architectures has been validated on SCANeR Studio simulator compared to an uncontrolled vehicle. Both the centralized and the decentralized architectures are relevant to control this complex system. It has been shown that the decentralized architecture is more simple to synthesize, while the centralized architecture handles more complex situations. From a research point of view, it seems that the centralized approach is stronger than the decentralized one especially because the global system closed-loop stability is theoretically provable. However, from an engineering point of view, the decentralized approach is more acceptable since it is more practical to develop sub-systems with local objectives, rather than thinking on the whole system where a lot of complexities arise. Besides, in general, more than one engineer work on the architecture, so that each of them can work on a part and then share blocks (model-based design approach). In other words, the engineering point of view is more realistic while the research point of view is more idealistic.
Future work will focus more on the other comparison criteria and a real-time implementation and validation of the proposed architectures will be performed on the platform being developed at Heudiasyc laboratory. Moreover, a Lyapunov-based theoretical study will be investigated to prove the stability of the decentralized architecture, and, the limits and conditions of its convergence. Investigations in chassis control will continue to tolerate possible faults on the ADAS actuators and to introduce more actuators. Learning based intelligent controllers should also be developed to improve the decision making process.

ACKNOWLEDGMENT

The authors would like to thank the Hauts-de-France Region and the European Regional Development Fund (ERDF) 2014/2020 for the funding of this work, through the SYSCOVI project. This work was also carried out in the framework of the Labex MS2T, (Reference ANR-11-IDEX-0004-02) and the Equipex ROBOTEX (Reference ANR-10-EQPX-44-01) which were funded by the French Government, through the program "Investments for the future" managed by the National Agency for Research.

References

R. Rajamani, *Vehicle Dynamics and Control*. Springer, 2012.

J. He, D. A. Crolla, M. Levesley, and W. Manning, "Coordination of active steering, driveline, and braking for integrated vehicle dynamics control," *Proceedings of the Institution of Mechanical Engineers, Part D: Journal of Automobile Engineering*, vol. 220, no. 10, pp. 1401–1420, 2006.

R. Karbalaei, A. Ghaffari, R. Kazemi, and S. Tabatabaei, "A new intelligent strategy to integrated control of afs/dyc based on fuzzy logic," *International Journal of Mathematical, Physical and Engineering Sciences*, vol. 1, no. 1, pp. 47–52, 2007.

C. Poussot-Vassal, O. Sename, and L. Dugard, "Robust vehicle dynamic stability controller involving steering and braking systems," in *IEEE European Control Conference (ECC), pp. 3646–3651*, 2009.

M. Doumiati, O. Sename, L. Dugard, J.-J. Martinez-Molina, P. Gaspar, and Z. Szabo, "Integrated vehicle dynamics control via coordination of active front steering and rear braking," *European Journal of Control*, vol. 19, no. 2, pp. 121–143, 2013.

M. Doumiati, A. Victorino, R. Talj, and A. Charara, "Robust lpv control for vehicle steerability and lateral stability," in *53rd IEEE Conference on Decision and Control, pp. 4113–4118*, 2014.

V. T. Vu, O. Sename, L. Dugard, and P. Gáspár, "Enhancing roll stability of heavy vehicle by lqr active anti-roll bar control using electronic servo-valve hydraulic actuators," *Vehicle System Dynamics*, vol. 55, no. 9, pp. 1405–1429, 2017.

J. Yao, G. Lv, M. Qv, Z. Li, S. Ren, and S. Taheri, "Lateral stability control based on the roll moment distribution using a semiactive suspension," *Proceedings of the Institution of Mechanical Engineers, Part D: Journal of Automobile Engineering*, vol. 231, no. 12, pp. 1627–1639, 2017.

M. Mirzaei and H. Mirzaeinejad, "Fuzzy scheduled optimal control of integrated vehicle braking and steering systems," *IEEE/ASME Transactions on Mechatronics*, vol. 22, no. 5, pp. 2369–2379, 2017.

O. Sename, P. Gaspar, and J. Bokor, *Robust control and linear parameter varying approaches: application to vehicle dynamics*. Springer, vol. 437, 2013.

W. Chen, H. Xiao, Q. Wang, L. Zhao, and M. Zhu, *Integrated vehicle dynamics and control*. John Wiley & Sons, 2016.

S. Fergani, O. Sename, and L. Dugard, "A new lpv/h global chassis control through load transfer distribution and vehicle stability monitoring," *IFAC Proceedings Volumes*, vol. 46, no. 2, pp. 809–814, 2013.

J. Ackermann and D. Odenthal, "Robust steering control for active rollover avoidance of vehicles with elevated center of gravity," *Citeseer*, 1998.

D. Odenthal, T. Bunte, and J. Ackermann, "Nonlinear steering and braking control for vehicle rollover avoidance," in *IEEE European Control Conference (ECC), pp. 598–603*, 1999.

S. Solmaz, M. Corless, and R. Shorten, "A methodology for the design of robust rollover prevention controllers for automotive vehicles with active steering," *International Journal of Control*, vol. 80, no. 11, pp. 1763–1779, 2007.

A. Chokor, R. Talj, A. Charara, H. Shraim, and C. Francis, "Active suspension control to improve passengers comfort and vehicle's stability," in *19th International Conference on Intelligent Transportation Systems (ITSC)*. IEEE, 2016, pp. 296–301.

A. Chokor, R. Talj, A. Charara, M. Doumiati, and A. Rabhi, "Rollover prevention using active suspension system," in *20th International Conference on Intelligent Transportation Systems (ITSC)*. IEEE, 2017, pp. 1706–1711.

M. Doumiati, A. Charara, A. Victorino, and D. Lechner, *Vehicle dynamics estimation using Kalman filtering: experimental validation*. John Wiley & Sons, 2012.

B. Heissing and M. Ersoy, *Chassis handbook: fundamentals, driving dynamics, components, mechatronics, perspectives*. Springer Science & Business Media, 2010.

D.-W. Gu, P. Petkov, and M. M. Konstantinov, *Robust control design with MATLAB®*. Springer Science & Business Media, 2005.

P. Apkarian, P. Gahinet, and G. Becker, "Self-scheduled h control of linear parameter-varying systems: a design example," *Automatica*, vol. 31, no. 9, pp. 1251–1261, 1995.

P. Apkarian and P. Gahinet, "A convex characterization of gain-scheduled h/sub/spl infin//controllers," *IEEE Transactions on Automatic Control*, vol. 40, no. 5, pp. 853–864, 1995.

C. Scherer, P. Gahinet, and M. Chilali, "Multiobjective output-feedback control via lmi optimization," *IEEE Transactions on automatic control*, vol. 42, no. 7, pp. 896–911, 1997.

V. Utkin, "On convergence time and disturbance rejection of super-twisting control," *IEEE Transactions on Automatic Control*, vol. 58, no. 8, pp. 2013–2017, 2013.

W. Klier, G. Reimann, and W. Reinelt, "Concept and functionality of the active front steering system," SAE Technical Paper, Tech. Rep., 2004.

6. Appendices

Appendix A. Yaw-roll coupled LTI model

$$
\begin{aligned}
a_{11} &= (c_1 + I_{xz} * d_1 * (1 + b_1))/(d_4 * I_z),\\
a_{12} &= (c_2 + I_{xz} * d_1 * b_2)/(d_4 * I_z),\\
a_{13} &= I_{xz} * d_2/(d_4 * I_z),\\
a_{14} &= I_{xz} * d_3/(d_4 * I_z),\\
a_{21} &= b_1 + M_s * h_\theta * a_{41}/(M * v),\\
a_{22} &= b_2 + M_s * h_\theta * a_{42}/(M * v),\\
a_{23} &= M_s * h_\theta * a_{43}/(M * v),\\
a_{24} &= M_s * h_\theta * a_{44}/(M * v),\\
a_{41} &= d_1 * (1 + b_1)/d_4,\\
a_{42} &= d_1 * b_2/d_4,\\
a_{43} &= d_2/d_4 + d_5 * a_{13},\\
a_{44} &= d_3/d_4 + d_5 * a_{14},
\end{aligned}
\tag{A1}
$$

$$
\begin{aligned}
b_{u,11} &= (c_\delta + I_{xz} * a_\delta/I_z)/c_4,\\
b_{u,21} &= b_\delta + M_s * h_\theta * b_{u,41}/(M * v),\\
b_{u,41} &= d_1 * b_\delta/d_4 + d_5 * b_{u,11},\\
b_{u,12} &= 1/(I_z * c_4),\\
b_{u,22} &= M_s * h_\theta * b_{u,42}/(M * v),\\
b_{u,42} &= d_5 * b_{u,12},
\end{aligned}
\tag{A2}
$$

$$
\begin{aligned}
b_{d,11} &= 1/I_z,\\
b_{d,22} &= 1/M_v,\\
b_{d,22} &= 1/I_z.
\end{aligned}
\tag{A3}
$$

where,

$$
\begin{aligned}
a_\delta &= d_1 * b_\delta/d_4,\\
b_\delta &= \mu * C_f/(M * v),\\
b_1 &= -1 + \mu * (C_r * l_r - C_f * l_f)/(M * v^2),\\
b_2 &= -\mu * (C_f + C_r)/(M * v),\\
c_\delta &= (1/I_z) * \mu * C_f * l_f,\\
c_1 &= -(1/I_z) * (\mu/v) * (C_f * (l_f^2) + C_r * l_r^2),\\
c_2 &= (1/I_z) * \mu * (C_r * l_r - C_f * l_f),\\
c_4 &= 1 - I_{xz} * d_5/I_z,\\
d_1 &= M_s * h_\theta * v/(I_x + M_s * h_\theta^2),\\
d_2 &= (M_s * h_\theta * g - K_\theta)/(I_x + M_s * h_\theta^2),\\
d_3 &= -C_\theta/(I_x + M_s * h_\theta^2),\\
d_4 &= 1 - d_1 * M_s * h_\theta/(M * v),\\
d_5 &= I_{xz}/((I_x + M_s * (h_\theta^2)) * d_4).
\end{aligned}
\tag{A4}
$$